

Dust attenuation in the restframe ultraviolet: constraints from star-forming galaxies at $z \sim 1$

Charlie Conroy

Department of Astrophysical Sciences, Princeton University, Princeton, NJ 08544, USA

6 February 2020

ABSTRACT

A novel technique is employed for estimating attenuation curves in galaxies where only photometry and spectroscopic redshifts are available. This technique provides a powerful measure of particular extinction features such as the UV bump at 2175\AA , which has been observed in environments ranging from the Milky Way to high-redshift star-forming galaxies. Knowledge of the typical strength of the UV bump is crucial for converting restframe UV flux into star formation rates, and yet there are surprisingly few observational constraints on this feature. The UV bump will impart a unique signature as it moves through various filters due to redshifting; its presence can therefore be disentangled from other stellar population effects. The utility of this technique is demonstrated with a large sample of galaxies drawn from the DEEP2 Galaxy Redshift Survey. The observed $B - R$ color of star-forming galaxies at $0.6 < z < 1.4$ disfavors the presence of a UV bump, and instead favors restframe UV ($1800\text{\AA} < \lambda < 3000\text{\AA}$) attenuation curves similar to the Milky Way without a UV bump or a power-law with index $\delta = -0.7$.

1 INTRODUCTION

Estimating the stellar masses, ages, and star formation rates of large samples of galaxies has become common thanks both to large homogeneous spectroscopic and photometric surveys and to increasingly accurate and sophisticated stellar population synthesis (SPS) models. These models rely on stellar evolution calculations, stellar spectral libraries, an initial stellar mass function, and accurate dust attenuation models. Unfortunately, each of these ingredients carry uncertainties that are large enough to significantly impact the derived physical properties (see e.g. Conroy et al. 2008, and references therein).

Accurate modeling of attenuation by dust is particularly challenging. It is common practice in SPS to constrain the dust opacity in the visible portion of the spectrum, and then adopt, with little justification, an attenuation curve¹ to infer the dust opacity at both shorter and longer wavelengths. Common assumptions for the wavelength dependence include a power-law: $\tau \propto \lambda^\delta$ with $\delta = -0.7$, (Charlot & Fall 2000), a parameterization advocated by Calzetti and collaborators (Calzetti et al. 1994, 2000), the extinction curves of the Milky Way and Magellanic Clouds (Cardelli et al. 1989; Fitzpatrick 1999), or attenuation curves derived via the combination of either the Milky Way or Magellanic

Cloud extinction curves with a variety of star-dust geometries (Witt & Gordon 2000; Gordon et al. 2001). An attenuation curve must be assumed — rather than self-consistently applied — because the dependence of dust properties on quantities such as metallicity, local UV radiation intensity, and local and large-scale star-dust geometry are not understood either observationally or theoretically with the precision required for SPS models (Draine 2003).

Direct constraints on attenuation curves come principally from two techniques. The first assumes that the intrinsic spectrum of a source, such as a star, quasar, supernova, or gamma ray burst (GRB), is known, and then the ratio between the observed and intrinsic spectrum provides a probe of the wavelength-dependent extinction. This method is commonly used to measure extinction in nearby galaxies where individual stars can be resolved. It has also been applied to high-redshift galaxies that by chance alignment are back-lit by GRBs (e.g. Elíasdóttir et al. 2009), to multiply lensed quasars (e.g. Motta et al. 2002), and supernovae (e.g. Riess et al. 1996).

The second technique relies on the identification of classes of galaxies with similar physical properties (such as star formation rates and metallicities) that differ only in dust content. Comparing dusty to dust-free galaxies in the same class then provides a measure of the net attenuation suffered by the stars within the class. This technique was used by Calzetti and collaborators to measure the attenuation curve of actively star-forming galaxies at low redshift (Calzetti et al. 1994). Variants of this technique have been applied more recently by Johnson et al. (2007a,b)

¹ Attenuation refers to the net loss of photons at a given wavelength, while extinction refers to the loss of photons due to either scattering or absorption. ‘Attenuation’ will also be used when referring to the general concept of the loss of photons due to dust.

to photometry of a large sample of low redshift galaxies, and Noll et al. (2009) who analyzed spectra of star-forming galaxies at $z \sim 2$.

The most striking feature of the extinction curves in the Milky Way and Large Magellanic Cloud is the strong, broad absorption feature at 2175\AA , the ‘UV bump’ (Stecher 1965). The carrier of this absorption feature has not been positively identified, though polycyclic aromatic hydrocarbons (PAHs) are a leading candidate (Weingartner & Draine 2001; Draine 2003). Curiously, there is little evidence of a UV bump through most sightlines in the SMC, and it appears to be absent from the net attenuation curves of local starburst galaxies (Calzetti et al. 1994, 2000). However, spectroscopy of a sample of star-forming galaxies at $z \sim 2$ shows evidence for this feature (Noll & Pierini 2005; Noll et al. 2009). Multiply lensed quasars and gamma-ray bursts, when used as probes of foreground galaxies, show varied results regarding the presence of the UV bump (Motta et al. 2002; Vijn et al. 2003; Wang et al. 2004; Mediavilla et al. 2005; York et al. 2006; Elíasdóttir et al. 2009).

The strength of the UV bump encodes unique information regarding the formation and destruction of dust grains and is therefore a useful probe of the interstellar medium (ISM) where the UV photons are being absorbed (Draine 2003). Explanations for the observed variance in the strength of the UV bump include metallicity dependence, the effects of complex star-dust geometry, and varying physical conditions of the ISM.

The observed variation in strength of the UV bump has interest beyond the ISM. UV flux is routinely used as a proxy for star formation in galaxies. The observed UV flux is corrected for dust attenuation via the adoption of an attenuation curve which, in most cases, do not include the UV bump. However, if this additional absorption feature is present in galaxies, omission of it in the adopted attenuation curve will result in a systematic underestimation of star formation rates. For example, the NUV, *u*, *B*, or *R* band filters at $z = 0.0, 0.6, 1.0$, or 2.0 , respectively, will be sensitive to the presence of this feature.

This Letter is dedicated to exploring the observational evidence for a strong absorption feature at 2175\AA in a large sample of star-forming galaxies at $z \sim 1$. Where necessary, a flat Λ CDM cosmology is assumed with the following parameters ($\Omega_m, \Omega_\Lambda, h$) = (0.24, 0.76, 0.72). All magnitudes are in the *AB* system (Oke & Gunn 1983), and stellar masses assume a Chabrier (2003) IMF.

2 TECHNIQUE

Imagine identifying the same, or statistically similar galaxies at a variety of redshifts. The flux through a fixed bandpass filter will then trace out the average spectral energy distribution (SED) of the sample because of redshifting. In effect, one is measuring the average SED for this set of galaxies convolved with the filter. As the UV bump moves into and out of a given filter, it will impart unique changes that, with the aid of models, can be separated from variations in the underlying continuum. This basic idea was exploited by Vijn et al. (2003) to conclude that average star-forming galaxies at $z \sim 2$ do not show evidence for a strong UV bump.

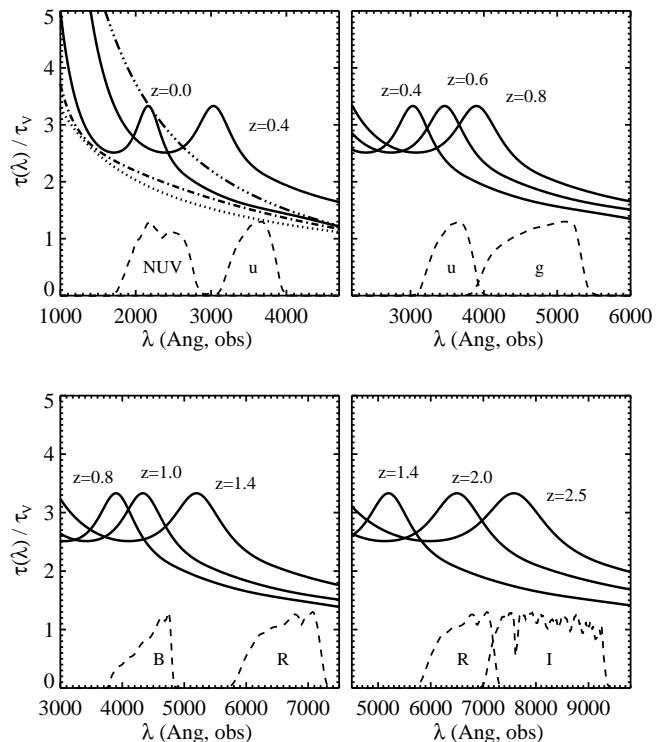


Figure 1. Average Milky Way extinction curve (solid lines), normalized to the *V*-band, as would be observed at various redshifts. Transmission curves (with arbitrary normalization; dashed lines) are included for common bandpass filters that would be sensitive to the presence of a UV bump. A power-law attenuation curve with index $\delta = -0.7$ (dotted line), $\delta = -1.3$ (dot-dot-dot-dashed line) and Calzetti attenuation (dot-dashed line) are included in the upper left panel. Note the different *x*-axis scales in each panel.

The challenging aspect of this approach is the requirement that one identifies the same, or similar galaxies at multiple epochs. This requirement is, however, relatively easy to satisfy in the restframe UV. As demonstrated in the following section, for typical star-forming galaxies the restframe UV is sensitive principally to dust attenuation and is not sensitive to other physical parameters such as total stellar mass or metallicity.

This technique is probing the spectrum of an average star-forming galaxy and therefore avoids several of the standard degeneracies between dust attenuation and SFR. In particular, the SFH of an average galaxy must be smooth, and one therefore cannot appeal to recent bursts of star formation in the interpretation of the restframe UV. Finally, note that this technique becomes conceptually cleaner at higher redshifts because at higher redshifts the redshift range over which the UV bump will move into and out of a given filter will correspond to a smaller change in lookback time. One may thus more confidently gather a statistically similar sample of galaxies over the requisite redshift range.

3 MODELS

This section describes the SPS model, including the prescription for attenuation by interstellar dust, used to generate SEDs of mock galaxies. The relation between attenuation curves and observed colors is explored, and a demonstration of the proposed technique is undertaken.

The SPS treatment closely follows that of Conroy et al. (2008), to which the reader is referred for details. The model includes all relevant phases of stellar evolution for metallicities in the range $10^{-4} < Z < 0.030$, for ages $10^{6.6} < t < 10^{10.2}$ yrs, and for initial masses $0.10 \leq M \leq 100 M_{\odot}$ (Marigo & Girardi 2007; Marigo et al. 2008). The initial stellar mass function (IMF) of Kroupa (2001) is adopted.

The fiducial dust model closely follows the two component model proposed by Charlot & Fall (2000). Stars younger than 10^7 years are subject to attenuation associated with their birth cloud. In addition, all stars experience attenuation due to diffuse, cirrus dust. These two sources of attenuation are parameterized by τ_1 and τ_2 , respectively, where τ is the optical depth at $\lambda = 5500\text{\AA}$. This two component model has strong observational motivation not only from direct observations of young stars embedded in molecular clouds but also from integrated spectra of star-forming galaxies, where the opacity measured in balmer emission lines is a factor of two larger than the opacity as measured from the stellar continuum (Calzetti et al. 1994). Charlot & Fall (2000) favor $\tau_1 = 1.0$ and $\tau_2 = 0.3$ based on a sample of low redshift star-forming galaxies. Unless stated otherwise, these will be the parameter choices used herein.

A second dust model is also considered, where a single screen of dust attenuates all starlight equally, independent of the age of the stars. This dust model is adopted when utilizing the Calzetti attenuation curve because this curve was derived by considering the net attenuation of all starlight, independent of stellar age. When employing this model, the single opacity characterizing the dust optical depth is equal to $1.5\tau_2$. The numerical coefficient was chosen to achieve a close correspondence in restframe UV colors between the two models.

An attenuation curve must be adopted to extrapolate the optical depth at 5500\AA to both shorter and longer wavelengths. A variety of commonly used curves are considered for the cirrus dust, including a power-law with index δ , a form advocated by Calzetti (2001), and the average extinction curve measured for the Milky Way, both with and without the UV bump at 2175\AA . Dust obscuration of young stars, characterized by τ_1 , is computed with a power-law attenuation curve with $\delta = -0.7$.

Figure 1 shows the Milky Way extinction curve as seen at various redshifts. The figure also shows the location of various common bandpass filters, and, in the top left panel, the attenuation curve of Calzetti et al. and power-law attenuation curves with index $\delta = -0.7$ and $\delta = -1.3$, for comparison. The purpose of this figure is to demonstrate at which epochs particular filters are sensitive to the presence of the UV bump. For example, at $z = 1.0$ the UV bump would be redshifted into the B -band, and so by considering the B -band flux of galaxies at $0.8 < z < 1.4$ one might hope to measure the strength of the UV bump.

The power of the proposed technique to constrain the average restframe ultraviolet attenuation curve is demon-

strated with mock galaxies. Each mock galaxy is assumed to be composed of stars of a single metallicity and with a star formation rate (SFR) characterized by a simple exponential: $\text{SFR} \propto e^{-t/\tau_{\text{SF}}}$ from $t = 0$ to the age of the universe at the redshift of the mock galaxy. Starlight is attenuated by dust according to the model described above.

The evolution of observed-frame $B - R$ colors with redshift is shown for mock galaxies in Figure 2. In this figure the sensitivity of the $B - R$ color evolution to various parameters is explored. It is clear that the color evolution is entirely insensitive to metallicity, and is only sensitive to the star formation history (SFH) for pathological values of τ_{SF} . Color evolution is most sensitive to the normalization of the attenuation curve, τ_2 and the attenuation curve itself. While not shown, the color evolution is also insensitive to τ_1 for $0.5 < \tau_1 < 1.5$.

4 DATA

Galaxies are drawn from the DEEP2 Galaxy Redshift Survey (Davis et al. 2003), which has gathered optical spectra for $\sim 40,000$ galaxies, primarily in the redshift range $0.7 < z < 1.4$. Target galaxies were selected using BRI imaging from the CFHT telescope down to a limiting magnitude of $R = 24.1$ (Coil et al. 2004). In three of the four fields observed colors are used to exclude objects likely to have $z < 0.7$; the sampling rate at $z < 0.7$ is thus 1/4 the rate at higher redshift. Redshift errors are $\sim 30 \text{ km s}^{-1}$ as determined from repeated observations. Details of the DEEP2 observations, catalog construction, and data reduction can be found in Davis et al. (2003), Coil et al. (2004), and Davis et al. (2005). Restframe $U - B$ colors and absolute B -band magnitudes, M_B , have been derived as described in Willmer et al. (2006). Stellar masses for a subset of DEEP2 galaxies were derived by Bundy et al. (2006). With these masses an empirically derived relation between rest-frame UBV colors and stellar mass was obtained in order to assign stellar masses to all DEEP2 galaxies (C.N.A. Willmer, private communication).

Star formation rates, metallicities, and V -band dust opacities are not readily available for all DEEP2 galaxies. Galaxies thus cannot be binned in these quantities as a function of redshift. Instead, two simple cuts are made to ensure that similar galaxies are selected across the redshift range. A cut on restframe $U - B$ color is made to exclude red sequence galaxies: $U - B < -0.032(M_B + 21.63) + 1.03$. A second cut is made on stellar mass, requiring $10.0 < \log(M/M_{\odot}) < 10.5$. Since stellar mass is correlated with SFR at $z \sim 1$ (Noeske et al. 2007), this cut corresponds, at least approximately, to a cut on SFR. Applying these cuts to the data leaves 4,203 galaxies in the redshift range $0.6 < z < 1.4$. The results presented in the following section are robust to the subsample of data used. For example, the conclusions are unchanged if all galaxies are included in the analysis.

5 RESULTS

The primary result of this Letter is contained in Figure 3. In this figure the variation in observed $B - R$ color with

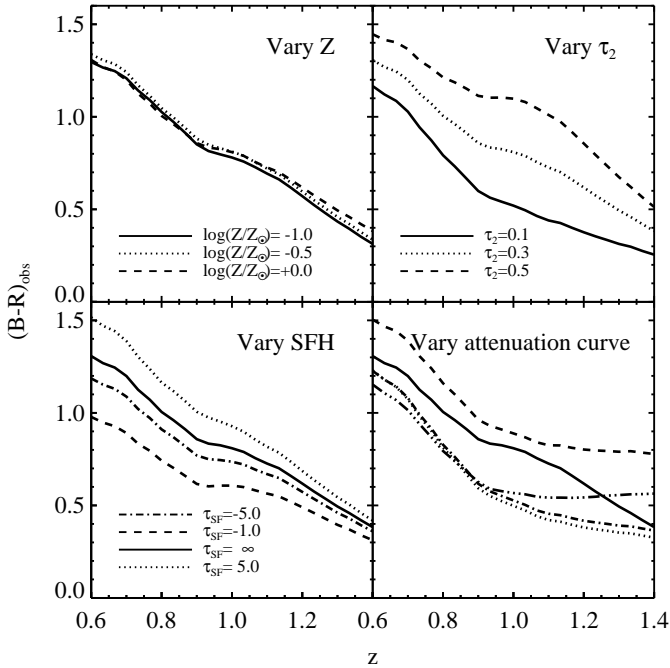


Figure 2. Observed-frame $B - R$ color as a function of redshift. In each panel one parameter is varied about the default values of $Z = Z_{\odot}$, constant SFH ($\tau_{\text{SF}} = \infty$), $\tau_2 = 0.3$, and a Milky Way extinction curve with a UV bump. The lower right panel shows the effect of varying the extinction curve between a power-law with an index of -1.3 (dashed line) and -0.7 (dot-dashed line), a Calzetti attenuation curve (dot-dot-dashed line), and Milky Way extinction curves with (solid line) and without (dotted line) a UV bump.

redshift for 4,203 DEEP2 galaxies is compared to the expected color evolution for a galaxy with solar metallicity and constant star formation rate. In the left panel the data are compared to expected colors for the default dust model parameter $\tau_2 = 0.3$, for three different attenuation curves: Milky Way extinction both with and without a UV bump, and Calzetti attenuation.

In the right panel attention is focused on models with Milky Way extinction curves both with and without the UV bump, for $\tau_2 = 0.1, 0.3, 0.5$. It is clear from this figure that the presence of the UV bump is strongly disfavored by the data, unless the typical galaxy at $z \sim 1$ has a V -band opacity of $\tau_2 \leq 0.1$. The latter possibility is highly unlikely given that typical V -band opacities for star-forming $\sim L^*$ galaxies are rarely lower than 0.2 both in the local universe and at higher redshift (for a review, see Calzetti 2001). If an attenuation curve with a UV bump is to be retained, then the distribution of $B - R$ colors at fixed redshift implies not only that the average τ_2 be ≤ 0.1 but that the distribution of τ_2 values must be very strongly peaked about the average value. This must be so in order for there to be so few data points above $B - R = 0.7$ at $z = 1.0$, for example. Such a scenario seems implausible.

This figure also demonstrates that the model using the Calzetti attenuation curve provides a relatively poor description of the data at $z > 1$. Whether or not this discrepancy is due to different star-dust geometries or different dust prop-

erties compared to low redshift star-forming galaxies is unclear.

Comparison of the lower right panel of Figure 2 with Figure 3 reveals several additional results. First, the Milky Way extinction curve without the UV bump is very similar to a power-law dust attenuation curve with index $\delta = -0.7$, at least over the restframe wavelengths probed in the figure. Therefore, power-law attenuation curves with $\delta = -0.7$ also agree well with the data. On the other hand, a power-law attenuation curve with $\delta = -1.3$ produces colors much redder than observed for $\tau_2 = 0.3$. Models with $\delta = -1.3$ and $\tau_2 = 0.1$ produce acceptable agreement with the data, but they are then subject to the same objections as raised above for the Milky Way extinction curve with the UV bump.

These results are not sensitive to the treatment of dust attenuation around young stars. Recall that the dust model associates additional dust obscuration around stars with ages $t < 10^7$ years. A power-law attenuation curve was adopted for these young stars. If instead a Milky Way extinction curve with a UV bump is adopted for all stars, including young ones, then the disagreement between the models and data is more severe. Furthermore, varying the V -band optical depth around young stars from $\tau_1 = 0.5$ to $\tau_1 = 1.5$ does not change these results. Varying the boundary between young and old stars from $10^{6.5}$ to $10^{7.5}$ years, or allowing for a fraction of ‘naked’ young stars that have escaped their birth clouds, shifts the model predictions by a constant amount in $B - R$ and therefore cannot help to reconcile the model predictions including a UV bump with the data. Finally, adopting a uniform dust screen, where all stars are subject to the same attenuation, only strengthens the result that there is no evidence for a UV bump in $z \sim 1$ star-forming galaxies.

It is important to remember that BR photometry at these epochs is probing restframe $1800\text{\AA} < \lambda < 3000\text{\AA}$. The results in this section concerning the attenuation curve therefore only apply to that wavelength range. It would therefore be unwise to extrapolate these results to longer or shorter wavelengths.

6 CONCLUSION

If the UV bump at restframe 2175\AA were a generic feature of extragalactic attenuation curves, then the observed-frame $B - R$ colors of galaxies should redden substantially as the UV bump redshifts into the B -band at $z = 1$, and then rapidly become bluer as this feature redshifts out of the band by $z = 1.4$. Comparison of simple models to the observed $B - R$ colors of galaxies over the redshift range $0.6 < z < 1.4$ reveals that the UV bump is not a ubiquitous feature in the observed SEDs of star-forming galaxies at $z \sim 1$. This is the principle result of this Letter.

A more general lesson to be drawn here is that dust attenuation curves need not be assumed, but instead can be directly constrained by the data, even when the data consist only of broadband photometry. It would be fruitful to repeat this exercise at both lower and higher redshifts, where the necessary data already exists. Stringent constraints on dust attenuation in the restframe ultraviolet for large samples of galaxies at a variety of epochs will not only afford a more robust transformation between UV flux and SFR, but may

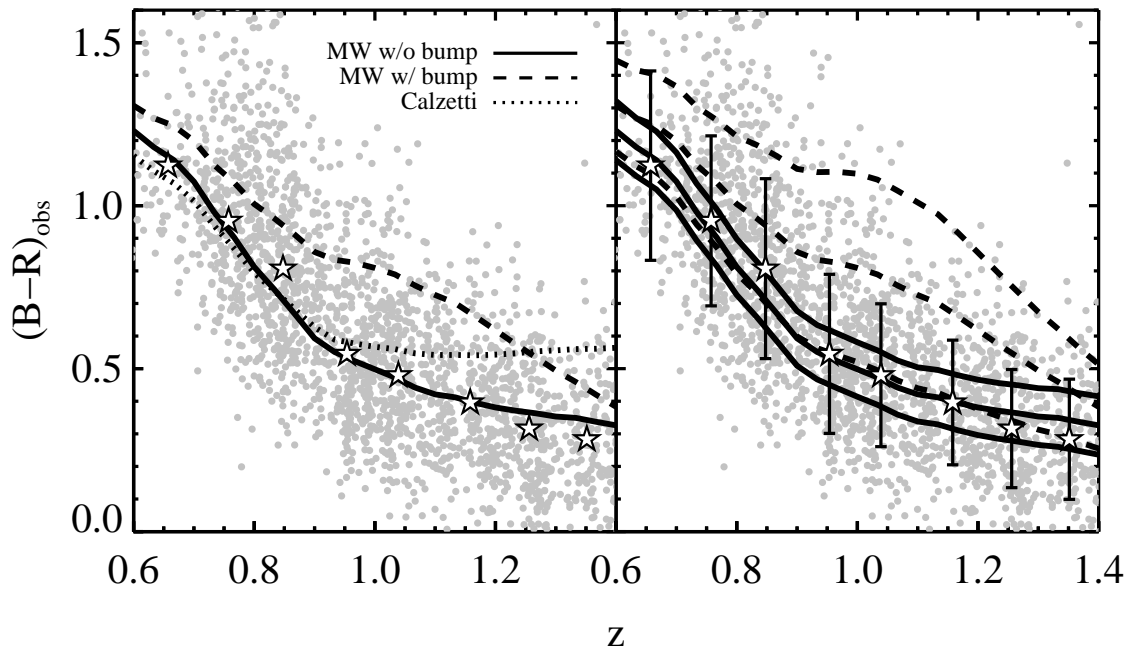


Figure 3. Observed-frame $B - R$ color as a function of redshift. Data are from the DEEP2 Survey (*solid grey circles*). Model predictions (*lines*) are compared to the average trend in the data (*stars*). Error bars denote 1σ scatter in the data. *Left panel:* Data are compared to model predictions for the standard set of assumptions ($\tau_2 = 0.3$, constant SFH, $Z = Z_\odot$), with three dust attenuation curves: Milky Way extinction with (*dashed line*) and without (*solid line*) the UV bump, and Calzetti attenuation (*dotted line*). *Right panel:* Data are compared to model predictions using Milky Way extinction curves with (*dashed lines*) and without (*solid lines*) the UV bump, for three values of the dust opacity: $\tau_2 = 0.1, 0.3, 0.5$ (*bottom, middle, and top lines*, respectively). The Milky Way extinction curve without a UV bump provides the best description of the data over a wide range in τ_2 , while the extinction curve with a UV bump only describe the trends in the data for unreasonably low values of τ_2 .

also shed light on dust properties and the relative distribution of stars and dust over a range of environments and epochs.

ACKNOWLEDGMENTS

It is a pleasure to thank Bruce Draine for numerous conversations related to this work, Jeffrey Newman for clarifying various data related issues and catching several errors in an earlier draft, and Christopher Willmer for providing his derived data products catalog. Funding for the DEEP2 survey has been provided by NSF grants AST95-09298, AST-0071048, AST-0071198, AST-0507428, and AST-0507483 as well as NASA LTSA grant NNG04GC89G. The data presented herein were obtained at the W. M. Keck Observatory, which is operated as a scientific partnership among the California Institute of Technology, the University of California and NASA. The Observatory was made possible by the generous financial support of the W. M. Keck Foundation. This work made extensive use of the NASA Astrophysics Data System and of the *astro-ph* preprint archive at [arXiv.org](http://arxiv.org).

REFERENCES

Bundy K., et al., 2006, *ApJ*, 651, 120
 Calzetti D., 2001, *PASP*, 113, 1449

Calzetti D., Armus L., Bohlin R. C., Kinney A. L., Koornneef J., Storchi-Bergmann T., 2000, *ApJ*, 533, 682
 Calzetti D., Kinney A. L., Storchi-Bergmann T., 1994, *ApJ*, 429, 582
 Cardelli J. A., Clayton G. C., Mathis J. S., 1989, *ApJ*, 345, 245
 Chabrier G., 2003, *PASP*, 115, 763
 Charlot S., Fall S. M., 2000, *ApJ*, 539, 718
 Coil A. L., et al., 2004, *ApJ*, 617, 765
 Conroy C., Gunn J. E., White M., 2008, *ArXiv:0809.4261*
 Davis M., Gerke B. F., Newman J. A., 2005, in *ASP Conf. Ser. 339: Observing Dark Energy*, Wolff S. C., Lauer T. R., eds., p. 128
 Davis M., et al., 2003, in *Proc. SPIE, Volume 4834*, pp. 161-172 (2003), pp. 161-172
 Draine B. T., 2003, *ARA&A*, 41, 241
 Elíasdóttir Á., et al., 2009, *ApJ*, 697, 1725
 Fitzpatrick E. L., 1999, *PASP*, 111, 63
 Gordon K. D., Misselt K. A., Witt A. N., Clayton G. C., 2001, *ApJ*, 551, 269
 Johnson B. D., et al., 2007a, *ApJS*, 173, 377
 —, 2007b, *ApJS*, 173, 392
 Kroupa P., 2001, *MNRAS*, 322, 231
 Marigo P., Girardi L., 2007, *AAP*, 469, 239
 Marigo P., Girardi L., Bressan A., Groenewegen M. A. T., Silva L., Granato G. L., 2008, *AAP*, 482, 883
 Mediavilla E., Muñoz J. A., Kochanek C. S., Falco E. E., Arribas S., Motta V., 2005, *ApJ*, 619, 749
 Motta V., Mediavilla E., Muñoz J. A., Falco E., Kochanek

- C. S., Arribas S., García-Lorenzo B., Oscoz A., Serra-Ricart M., 2002, *ApJ*, 574, 719
Noeske K. G., et al., 2007, *ApJL*, 660, L43
Noll S., Pierini D., 2005, *AAP*, 444, 137
Noll S., et al., 2009, *ArXiv:0903.3972*
Oke J. B., Gunn J. E., 1983, *ApJ*, 266, 713
Riess A. G., Press W. H., Kirshner R. P., 1996, *ApJ*, 473, 588
Stecher T. P., 1965, *ApJ*, 142, 1683
Vijh U. P., Witt A. N., Gordon K. D., 2003, *ApJ*, 587, 533
Wang J., Hall P. B., Ge J., Li A., Schneider D. P., 2004, *ApJ*, 609, 589
Weingartner J. C., Draine B. T., 2001, *ApJ*, 548, 296
Willmer C. N. A., et al., 2006, *ApJ*, 647, 853
Witt A. N., Gordon K. D., 2000, *ApJ*, 528, 799
York D. G., et al., 2006, *MNRAS*, 367, 945